Insight into the performance of GGA functionals for solid-state calculations

Philipp Haas, Fabien Tran, Peter Blaha, Karlheinz Schwarz, and Robert Laskowski
Institute of Materials Chemistry, Vienna University of Technology, Getreidemarkt 9/165-TC, A-1060 Vienna, Austria
(Received 24 August 2009; revised manuscript received 12 October 2009; published 12 November 2009)

Many exchange-correlation functionals of the generalized gradient approximation (GGA) are available in the literature. More particularly, during the last few years several research groups have proposed GGA functionals for solids, which very often perform better (especially for the lattice constant) than the standard GGA functional of Perdew, Burke, and Ernzerhof (PBE) [J. P. Perdew, K. Burke, and M. Ernzerhof, Phys. Rev. Lett. **77**, 3865 (1996)]. The improvement over PBE is not systematic, but trends among the different classes of solids can be observed [P. Haas, F. Tran, and P. Blaha, Phys. Rev. B **79**, 085104 (2009)]. A better understanding of the trends obtained with the existing functionals can obviously be very helpful for the construction of more accurate functionals, and in the aim of this we studied the distribution of the Wigner-Seitz radius r_s (related to the electron density ρ) and the reduced density gradient s in a few selected solids and identified the relevant ranges of r_s ($r_s<4$) and s ($s<2$) in solids. We focus on the variation of the exchange-correlation energy with respect to the unit-cell volume ($dE_{xc}/d\Omega$), which determines the equilibrium lattice constant and identify the "important regions" in the unit cell, where the differences of $dE_{xc}/d\Omega$ between two functionals are most pronounced. In metallic systems, these important regions coincide with the spatial separation of semicore and valence electrons, while for semiconductors (open structures) and insulators (inhomogeneous systems) the tails of the valence electrons become equally important or even dominate.

DOI: 10.1103/PhysRevB.80.195109 PACS number(s): 71.15.Mb, 71.15.Nc

I. INTRODUCTION

The Kohn-Sham version of density-functional theory[1,2] is the most common method for the calculation of the electronic properties of molecules and solids. Its success relies on the fact that the system of interacting electrons is mapped to a system of fictitious noninteracting electrons with the same electron density, i.e., the equations to solve are one-electron Schrödinger equations, and therefore very large systems can be calculated with a relatively low cost/accuracy ratio. Within the Kohn-Sham method,[2] the total energy of a system of electrons is given by (all equations are given in atomic units)

$$E_{\text{tot}} = T_s + \int v_{\text{ext}}(\mathbf{r})\rho(\mathbf{r})d^3r + \frac{1}{2}\int\int \frac{\rho(\mathbf{r})\rho(\mathbf{r}')}{|\mathbf{r}-\mathbf{r}'|}d^3r d^3r' + V_{\text{nn}} + E_{xc}, \quad (1)$$

where T_s is the kinetic energy of a system of noninteracting electrons, the three next terms represent the electron-nucleus, electron-electron, nucleus-nucleus electrostatic energies, and E_{xc} is the exchange-correlation energy which can be decomposed into its exchange and correlation parts ($E_{xc}=E_x+E_c$).

For calculations which are done using an accurate solution of the Kohn-Sham equations (e.g., all-electron treatment, no approximation for the potential, and large flexible basis set), the accuracy of the results depends solely on the quality of the approximation used for E_{xc}. The exact mathematical form of the exchange energy E_x is known (it is the same as in Hartree-Fock theory), but it is a functional which depends explicitly on the orbitals ψ_i and leads to calculations which are relatively expensive, especially for solids. For the correlation E_c, no exact form exists which can be used for practical calculations, and calculations using an accurate *ab initio* correlation functional (e.g., derived from perturbation theory) are very rare and expensive (see, e.g., Refs. 3 and 4). Nowadays, the standard functionals for calculations on molecular systems are the hybrid functionals.[5] These functionals, which consist of a mixture of Hartree-Fock and semilocal exchange (and are intrinsically empirical[6]), are very good for the structural and thermochemical properties of molecules. Nevertheless, new types of functionals yielding promising results are continued to be proposed (see, e.g., Refs. 6–10). For solids, the hybrid functionals do not constitute the standard choice, and only recently papers reporting extensive tests of hybrid functionals on solids have appeared (see, e.g., Refs. 11–13). The hybrid functionals often perform well, in particular (due to the potential which is orbital dependent) for the calculation of band gaps[12,13] for which the use of the local-density approximation (LDA) (Ref. 2) or generalized gradient approximation (GGA) is not appropriate due to the local nature of these approximations.[14] However, we mention two drawbacks of hybrid functionals for solids: their inadequacy for metallic systems[13,15] and the high cost, which is required for the evaluation of the Hartree-Fock energy and potential for solids. Thus, the LDA and GGA functionals remain the most widely used functionals in the solid-state community, where real materials science problems can require unit cells containing several hundreds of atoms.

The first GGA functional that has been used extensively for solids is PW91.[16] It has been replaced by PBE,[17] which until now has been the standard functional for calculations of solids. PBE belongs to the class of *parameter-free* functionals, i.e., it does not contain any parameter that was determined in order to reproduce experimental or accurate *ab initio* data. However, very recently several GGA functionals were proposed by different research groups, and some of them were especially designed to work well for the geometry of solids.[18–24] In Refs. 25–29 it has been shown that these functionals lead to very small signed mean error, indicating

that the typical underestimation (overestimation) of LDA (PBE) functionals has been significantly reduced. However, the improvement is not systematic, but trends among the different classes of compounds have been observed.[25,28] We also mention the functionals of the meta-GGA approximation,[30–32] which are more flexible due to the use of the kinetic-energy density. In particular, the recently proposed functional revTPSS of Perdew *et al.*[32] was shown to give excellent results for molecules and solids.

In the present work we have studied the distribution of the electron density and the reduced density gradient in several solids and determined which region of space is energetically important for the lattice constant. The enhancement factors (see below for the definition) of the considered GGA functionals will be studied in detail. We note that previous analyses of GGA functionals can be found in Refs. 29 and 33–40, which will be briefly summarized in the last section of this work.

The paper is organized as follows. In Sec. II, the studied functionals are described. In Sec. III, a detailed analysis of the electron-density distribution and of the performance of the functionals for a few selected solids is given. In Sec. IV, additional discussions and the summary of our work are given.

II. FUNCTIONALS

In this section, a short summary of the ideas behind the construction of the functionals and their performances is given.

A. LDA

The LDA functional has the following form:

$$E_{xc}^{\mathrm{LDA}}[\rho] = \int \epsilon_{xc}^{\mathrm{LDA}}(\rho(\mathbf{r}))d^3r, \tag{2}$$

where the exchange-correlation energy per volume unit $\epsilon_{xc}^{\mathrm{LDA}}$ is a function of the electron density ρ and is usually chosen to be the one of the uniform electron gas. The exchange part is given by $\epsilon_x^{\mathrm{LDA}} = -(3/4)(3/\pi)^{1/3}\rho^{4/3}$.[41] For the correlation part we chose the functional PW92,[42] which is one of the most accurate fits of quantum Monte Carlo data of the uniform electron gas.[43] This functional yields relatively good results for the geometry of solids and is still among the best for some classes of solids, e.g., the 5*d*-transition metals (see, e.g., Refs. 25, 27, and 28), but it fails badly for the atomization energies of molecules and solids.

B. GGA

For a better description of inhomogeneous systems, in particular atoms and molecules, the use of the gradient of the electron density revealed to be very helpful. This has led to the development of functionals of the so-called GGA family,

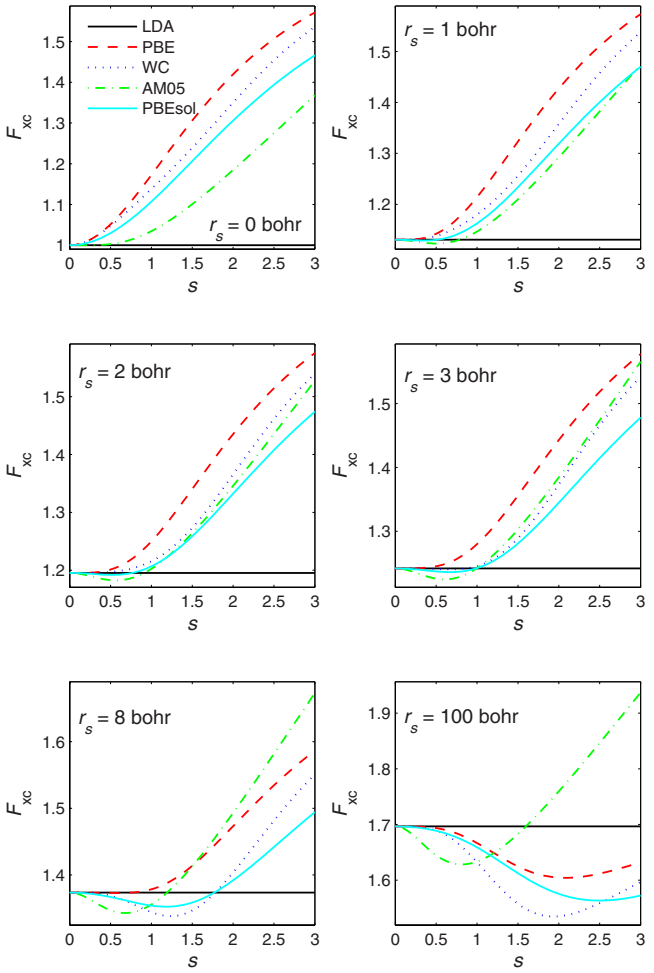

FIG. 1. (Color online) Enhancement factors F_{xc} plotted against the reduced density gradient s for different values of r_s. The horizontal line corresponds to LDA.

$$E_{xc}^{\mathrm{GGA}}[\rho] = \int \epsilon_{xc}^{\mathrm{GGA}}(\rho(\mathbf{r}), \nabla\rho(\mathbf{r}))d^3r$$
$$= \int \epsilon_x^{\mathrm{LDA}}(r_s(\mathbf{r}))F_{xc}(r_s(\mathbf{r}), s(\mathbf{r}))d^3r, \tag{3}$$

where $F_{xc}(r_s,s) = F_x(s) + F_c(r_s,s)$ is the enhancement factor, $r_s = [3/(4\pi\rho)]^{1/3}$ is the Wigner-Seitz radius, and $s = |\nabla\rho|/[2(3\pi^2)^{1/3}\rho^{4/3}]$ is the reduced density gradient. PW86,[44,45] BLYP,[46,47] and PW91 (Ref. 16) are the first GGA functionals which have been used extensively for practical calculations. In the literature, two classes of GGA functionals can be found: (a) the *empirical* functionals, whose parameters were determined by fitting experimental or *ab initio* data (see, e.g., Ref. 48), and (b) the parameter-free functionals, whose parameters were determined in order to satisfy mathematical relations which are known to hold for the exact functional (see, e.g., Ref. 17). However, it should be noted that all parameter-free functionals still contain arbitrary choices such as the analytical form chosen to represent F_{xc} or the choice of constraints that are satisfied. In Fig. 1 we show

the enhancement factor F_{xc} of the functionals considered in this work as a function of s for several values of r_s.

1. PBE

The PBE functional is nowadays the most commonly used functional for solid-state calculations. It was designed to satisfy several conditions that are obeyed by the exact functional and it contains no empirical parameters.[17] In most cases, PBE gives similar results as PW91 (Ref. 16) (its predecessor), but it has a simpler analytical form. Some of the conditions satisfied by PBE are the correct uniform electron gas limit (i.e., LDA is recovered when $s=0$), the Lieb-Oxford bound ($E_x \geq E_{xc} \geq -1.679 \int \rho^{4/3} d^3r$),[49] and the LDA linear response. The enhancement factor for exchange is given by

$$F_x^{\mathrm{PBE}}(s) = 1 + \kappa - \frac{\kappa}{1 + \frac{\mu}{\kappa} s^2}, \tag{4}$$

where $\kappa=0.804$ and $\mu=0.219\,51$. Note that μ is approximately two times larger than the value $\mu_{\mathrm{GE}}=10/81$ derived from the second-order gradient expansion (GE) of the exchange energy at the limit of a slowly varying electron density.[50] At this limit, the behavior of the correlation functional is determined by the parameter β, which has the value $\beta=\beta_{\mathrm{GE}}=0.0667$ (the second-order coefficient of the gradient expansion of the correlation energy). Since μ and β are related by $\mu=\beta\pi^2/3$, PBE satisfies the LDA linear response.[17] For values of r_s and s, which are relevant for solids around the equilibrium geometry ($r_s, s \lesssim 3$), F_{xc}^{PBE} is the largest enhancement factor among the considered GGAs (see Fig. 1). A good feature of the PBE functional is that it performs equally well for finite and infinite systems. Concerning the lattice constant of solids, there are GGA functionals (see below) which, on average, perform better than PBE. Nevertheless, there are classes of solids for which PBE remains the best (e.g., solids containing $3d$-transition elements[25,27,28]). In the meantime, many other GGA functionals have been proposed, which modified the PBE functional form either by simply changing the values of the parameters[20,23,51–54] or by modifying the mathematical form of Eq. (4).[19,21,22,24,55–57] Note that already in 1986, Becke proposed an exchange enhancement factor given by Eq. (4), but with $\kappa=0.9672$ and $\mu=0.2351$.[58]

2. WC

Wu and Cohen (WC) (Ref. 19) proposed a GGA exchange functional (used in combination with PBE correlation functional) that was shown to improve over LDA, PBE, and the meta-GGA TPSS (Ref. 31) for the equilibrium volume and bulk modulus of solids and to yield jellium surface exchange energies which are as accurate as TPSS values. The good performance of the WC functional for the lattice constant of solids was later confirmed using much larger sets of solids,[25,28] but it was also shown that it slightly worsens the atomization energies of molecules with respect to PBE.[25] The WC exchange enhancement factor is given by

$$F_x^{\mathrm{WC}}(s) = 1 + \kappa - \frac{\kappa}{1 + \frac{x(s)}{\kappa}}, \tag{5}$$

where $\kappa=0.804$ (same as PBE) and

$$x(s) = \frac{10}{81} s^2 + \left(\mu - \frac{10}{81}\right) s^2 e^{-s^2} + \ln(1 + c s^4), \tag{6}$$

where $\mu=0.219\,51$ (same as PBE) and $c=0.007\,932\,5$. For all values of s, $F_x^{\mathrm{WC}} \leq F_x^{\mathrm{PBE}}$ (see Fig. 1), but by construction F_x^{PBE} and F_x^{WC} have the same behavior for $s \to 0$ and $s \to \infty$. Note that Wu and Cohen wrongly claimed (see the comment on Ref. 19 and the reply) that $x(s)$ recovers the fourth-order parameters of the fourth-order gradient expansion of the exact exchange functional in the limit of a slowly varying density.[59] Their error is due to an misinterpretation of Eq. (7) in Ref. 31.

3. PBEsol

This functional has the same analytical form as the PBE functional, but the value of two parameters were changed in order to satisfy other conditions.[20] The value of μ [Eq. (4)] was set to $\mu=\mu_{\mathrm{GE}}=10/81$ to satisfy the second-order gradient expansion of the exchange energy, while in correlation, β (see Sec. II B 1) was chosen in order to reproduce the accurate TPSS values of the surface exchange-correlation energy of jellium (as done previously for the AM05 functional; see Sec. II B 4). This leads to an enhancement factor F_{xc}^{PBEsol}, which is closer to LDA than the PBE and WC enhancement factors (see Fig. 1) are. Actually, PBEsol was designed to be more accurate than PBE for solids and surfaces,[20] which has been confirmed for solids by several studies.[22,23,27–29] However, since $\mu=\mu_{\mathrm{GE}}$, PBEsol performs badly for the thermochemistry of molecules and solids[21,22,29] for which a value of $\mu \sim 2\mu_{\mathrm{GE}}$ is more appropriate.[21,29,60]

4. AM05

While many GGAs were constructed by fitting parameters to experimental data or by satisfying universal mathematical conditions, the AM05 functional[18,61] was developed by combining functionals from different model systems [the uniform electron gas (LDA) and the local Airy approximation (LAA) (Ref. 62)]. They are merged using an index (X) for taking the local nature of the system into account. For bulklike regions (small values of s), LDA is used, while for surfacelike regions (large values of s), the LAA functional is used. The exchange and correlation energies per unit volume are given by

$$\epsilon_x^{\mathrm{LAA}}(\rho,s) = \epsilon_x^{\mathrm{LDA}}(\rho)\{X(s) + [1 - X(s)] F_x^{\mathrm{LAA}}(s)\}, \tag{7}$$

$$\epsilon_c^{\mathrm{LAA}}(\rho,s) = \epsilon_c^{\mathrm{LDA}}(\rho)\{X(s) + [1 - X(s)]\gamma\}, \tag{8}$$

where $\gamma=0.8098$ and $X(s)=1-\alpha s^2/(1+\alpha s^2)$ with $\alpha=2.804$ (α and γ were fitted to the exchange-correlation surface energy of the jellium model). The analytical form of F_x^{LAA} can be found in Ref. 18. From Fig. 1, we can see that the AM05 enhancement factor is clearly different from the other GGAs

TABLE I. Equilibrium lattice constant a_0 (in Å) for Li, V, FeAl, Si, and LiF, and c_0 for graphite (Ref. 28). The references for the experimental values can be found in Ref. 28.

Method	Li	V	FeAl	Si	LiF	Graphite
LDA	3.363	2.932	2.812	5.407	3.911	6.7
PBEsol	3.433	2.963	2.840	5.438	4.006	7.3
WC	3.449	2.965	2.843	5.437	4.012	9.6
AM05	3.456	2.961	2.839	5.439	4.038	>15
PBE	3.435	3.001	2.869	5.475	4.068	8.8
Expt.	3.451	3.024	2.882	5.415	3.960	6.71

considered in this work. For $r_s=0$ bohr (i.e., exchange only), F_x^{AM05} is the lowest one until $s\sim 4.5$, while for s larger than ~ 5 it is the largest. Actually, $F_x^{\mathrm{AM05}}\to\infty$ for $s\to\infty$ (thus, the Lieb-Oxford bound is not satisfied). From Fig. 1 we can also see that with increasing r_s the crossings between F_{xc}^{AM05} and the other enhancement factors tend to values around $s=1-1.5$. Originally, this functional was designed to perform well for systems with surfaces,[18] but very recently it has been shown to be, on average, more accurate than PBE for the lattice constant for many classes of solids[26–29] and as accurate as the WC, PBEsol, and SOGGA (Ref. 21) functionals.[28]

III. ANALYSIS

In this section, the spatial distribution of r_s (related to the electron density ρ) and s (related to the gradient of the electron density $\nabla\rho$) and the exchange-correlation energy E_{xc} are analyzed in detail for a few selected solids. The solids are lithium [bcc ($A2$)], vanadium [bcc ($A2$)], and FeAl [cesium chloride ($B2$)] as examples for simple and $3d$ metals and an intermetallic compound; silicon [diamond ($A4$)] and LiF [sodium chloride ($B1$)] representing semiconductors and ionic systems, respectively; and graphite [hexagonal ($A9$)] whose hexagonal layers are weakly bound. The theoretical and the experimental equilibrium lattice constants of these systems (shown in Table I) were taken from Ref. 28. In the case of graphite, the in-plane lattice constant was kept fixed at the experimental value of 2.464 Å, i.e., only the interlayer distance c was optimized. The experimental values of the cubic systems were corrected for the zero-point anharmonic expansion (see Refs. 28, 63, and 64 for details). From Table I we can see that, for all systems except Li and graphite, LDA and PBE give the smallest and largest lattice constants, respectively, while for Li and graphite the WC and AM05 lattice constants are larger than the PBE ones.

Regarding the trends observed in the lattice constants for these solids, in the following we will try to answer questions like: (a) why does the functional $F1$ yield a lattice constant that is larger than the one calculated with functional $F2$, (b) what are the regions in space which are energetically important for the lattice constants, and (c) which values of r_s and s are relevant in solids. Since the enhancement factor of GGA functionals [see Eq. (3)] depends on r_s and s, an analysis of these two quantities can certainly help us to understand the behavior and performance of GGA functionals. However, as discussed in detail below, it is particularly important to consider the variations of r_s, s, and E_{xc} with respect to the unit-cell volume Ω. Actually, $dE_{xc}/d\Omega$ is the quantity that is directly related to the value of the equilibrium lattice constant.

For our analysis we will consider averages of r_s and s over a certain region in space defined as follows:

$$\bar{f}=\frac{1}{V}\int_V f(\mathbf{r})d^3r, \tag{9}$$

where $f=r_s$ or s, and V is the volume of, e.g., the unit cell or an atomic sphere. Defining $\bar{r}_s$ and $\bar{s}$ with Eq. (9) makes sense only for solids with a finite unit cell, while for molecular systems these averages are zero if V represents the whole space. Note that, in Refs. 34–37, an energy-weighted definition for $\bar{r}_s$ and $\bar{s}$ was used.

The calculations were done with the WIEN2K code[65] which solves the Kohn-Sham equations using the full-potential (linearized) augmented plane-wave and local orbitals [FP-(L)APW+lo] method.[66–68] The integrations in the Brillouin zone were done with a $\mathbf{k}$ mesh of $21\times21\times21$ for the cubic solids and $13\times13\times5$ for graphite. A value between 8 and 10 was chosen for $R_{\mathrm{MT}}^{\mathrm{min}}K_{\mathrm{max}}$ (the product of the smallest atomic sphere radius R_{MT} and the plane-wave cutoff parameter K_{max}), which determines the size of the basis set.

An important detail concerning the way the analysis is done is the following. For all solids in Table I except graphite, we checked that the lattice constant given by a specific functional is insensitive to self-consistency effects, i.e., for the evaluation of the total energy it hardly matters whether the electron density stems from the corresponding potential or from another one (in all cases, the change in the lattice constant is less than 0.001 Å). Thus, for these solids we have simplified the analysis and used the same electron density (the one obtained from the PBE potential) for the comparison of the exchange-correlation energies obtained by different functionals and the figures. In particular, it means that the difference in total energy between two functionals $F1$ and $F2$ is given only by the difference in the exchange-correlation energy,

$$E_{\mathrm{tot}}^{F1}-E_{\mathrm{tot}}^{F2}=E_{xc}^{F1}-E_{xc}^{F2}. \tag{10}$$

Concerning graphite (Sec. III F), the potential-energy curves were obtained from self-consistent calculations and the PBE electron density was used for the figures showing r_s and s.

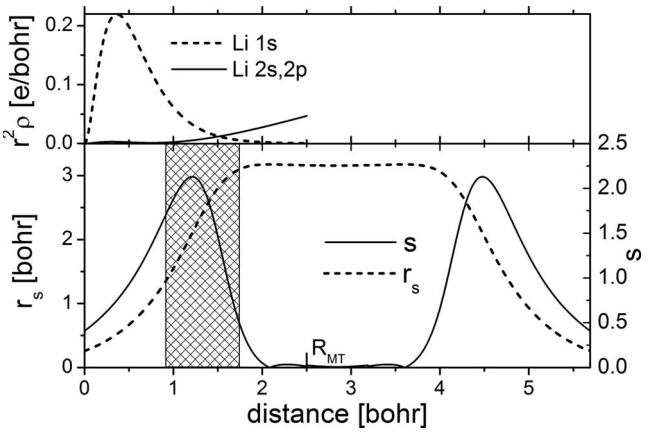

FIG. 2. Top: $r^2\rho$ of $1s$ (semi)core and $2s,2p$ valence states in bcc lithium (inside the atomic sphere). Bottom: r_s and s along the $(0,0,0)\rightarrow(1/2,1/2,1/2)$ path at the equilibrium volume. The important region (see text for definition) is illustrated by a hatched rectangle from 0.93 to 1.74 bohr and the atomic sphere radius ($R_{\mathrm{MT}}^{\mathrm{Li}}$) of the atom at 0 is indicated by a line at 2.5 bohr.

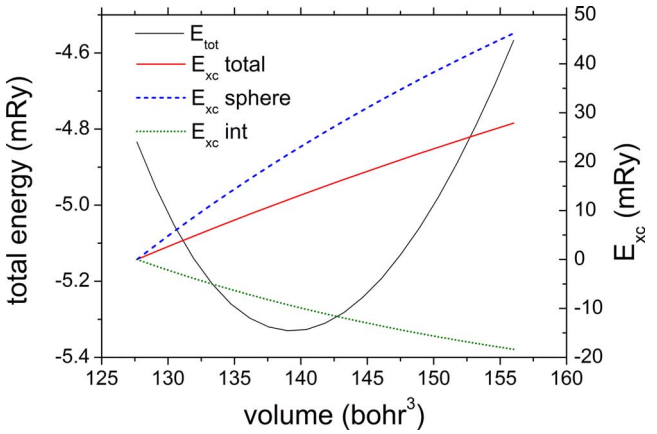

FIG. 3. (Color online) Variation of the total and exchange-correlation energies of lithium with respect to the unit-cell volume Ω (AM05 functional with PBE electron density). E_{xc} has been split into its contribution coming from the atomic sphere and the interstitial region. E_{tot}, E_{xc}^{total}, E_{xc}^{sphere}, and E_{xc}^{int} are shifted by 14.87, 3.57, 3.37, and 0.20 Ry, respectively.

A. Lithium

As a first example we analyze the simple metal Li in the bcc structure. Figure 2 shows the distribution of r_s and s along the cubic unit-cell diagonal at the equilibrium volume. In the interstitial region ($2<\mathrm{distance}<3.5$ bohr) s is basically zero and therefore only negligible differences between LDA and the various GGAs are expected in this region, since they all reduce to LDA for $s=0$. Inside the atomic sphere, the averages of r_s and s are about 2.66 bohr and 0.56, respectively, and, by looking at the enhancement factors (Fig. 1), we would expect PBEsol, WC, and AM05 functionals to yield lattice constants which are in between the LDA and PBE values. However, this is not the case (Table I): AM05 and WC lattice constants are larger than the PBE value. Therefore, a simple comparison of F_{xc} (as sometimes done) obviously does not explain the observed equilibrium lattice constants. A more detailed analysis is necessary in order to understand these trends.

The total and the exchange-correlation energies are plotted against the unit-cell volume Ω in Fig. 3. Although the contribution from E_{xc} to the total energy is relatively small, it is this small contribution that determines the lattice constant. We can also see that the variation of E_{xc} with respect to Ω is two orders of magnitude larger than for the total energy. Actually, it is the slope $dE_{xc}/d\Omega$ (and not the magnitude of E_{xc}) that determines the equilibrium geometry.

In Table II we show the values of $\Delta E_{xc}/\Delta\Omega=[E_{xc}(\Omega_2)-E_{xc}(\Omega_1)]/(\Omega_2-\Omega_1)$, where $E_{xc}(\Omega_1)$ and $E_{xc}(\Omega_2)$ are the exchange-correlation energies at the smallest (Ω_1) and largest (Ω_2) considered unit-cell volumes, respectively. $\Delta E_{xc}/\Delta\Omega$ is a good approximation to the slope $dE_{xc}/d\Omega$, which is nearly a linear function of Ω (see Fig. 3). As expected, these slopes reflect perfectly the trends observed in the lattice constants of Li: LDA leads to the largest slope and thus the smallest lattice constant, while AM05 has the smallest slope and thus the largest lattice constant. The PBE and PBEsol values, which are very similar, are in between.

The next step is to study the spatial decomposition of E_{xc}. Figure 3 shows the contributions to E_{xc} coming from the integration inside the atomic sphere ($R_{\mathrm{MT}}^{\mathrm{Li}}=2.5$ bohr) and the interstitial region.

The major contribution to E_{xc} comes from inside the atomic sphere, whereas the contribution from the interstitial region is an order of magnitude smaller due to the low density. However, for equilibrium lattice constants, we are interested (as mentioned before) in the change of E_{xc} with respect to the unit-cell volume Ω. From Fig. 3 we can see that the large linear increase inside the atomic sphere is partially canceled by the interstitial contribution.

Let us now investigate the difference between the slopes $\Delta E_{xc}/\Delta\Omega$ of two functionals $F1$ and $F2$. This difference is negligible in the interstitial region, which is easy to understand from Fig. 2. We see the clear minimum of r_s at the position of the atoms, but a rather constant value of r_s in the interstitial region, which shows the free-electron-like behavior of Li and originates from the superposition of the diffuse valence-electron densities of the atomic sites. Consequently, s is nearly zero in the interstitial region, which explains why this region does not contribute to the difference in slope $\Delta E_{xc}/\Delta\Omega$ between two GGA functionals that both reduce to LDA for $s=0$.

In order to make a more detailed study of $\Delta E_{xc}/\Delta\Omega$ inside the atomic sphere, we varied the limit r_{max} of the radial in-

TABLE II. Values (in mRy/bohr^3) of the slope $\Delta E_{xc}/\Delta\Omega$ (see text for definition) for Li and V.

Functional	Li	V
LDA	1.05	11.40
PBEsol	1.00	10.98
WC	0.99	10.95
AM05	0.98	11.00
PBE	1.00	10.50

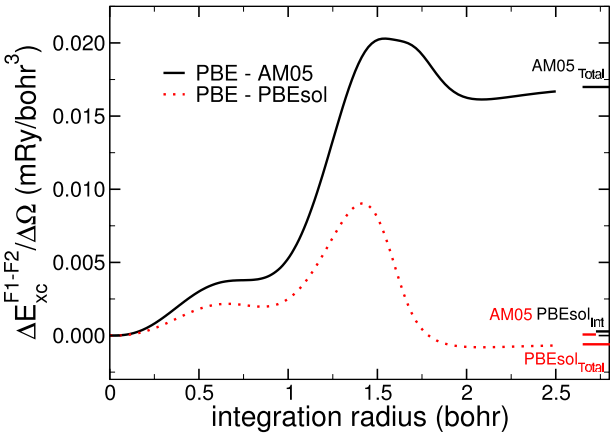

FIG. 4. (Color online) $\Delta E_{xc}^{F1-F2}(r_{\max})/\Delta\Omega$ for lithium with $F1$ =PBE and $F2$=AM05 (solid line) and $F1$=PBE and $F2$=PBEsol (dotted line) plotted as a function of the integration radius $r_{\max}$. The values of $\Delta E_{xc}^{F1-F2}/\Delta\Omega$ in the interstitial region and the whole unit cell are indicated by "Int" and "Total," respectively.

tegration. This allows us to identify which region around the nucleus is the most important for the determination of the equilibrium lattice constant. The function $\Delta E_{xc}^{F1-F2}(r_{\max})/\Delta\Omega = \Delta E_{xc}^{F1}(r_{\max})/\Delta\Omega - \Delta E_{xc}^{F2}(r_{\max})/\Delta\Omega$ approximates the difference in the slope of E_{xc} with volume for two functionals $F1$ and $F2$ as a function of the integration radius $r_{\max}$. In Fig. 4 we can see that the largest difference in the slope $\Delta E_{xc}/\Delta\Omega$ between the functionals $(F1,F2)$ =(PBE,AM05) or $(F1,F2)$=(PBE,PBEsol) originates from within a distance of about 1–1.75 bohr from the nucleus. Similar plots for other combinations with PBE have been analyzed and led us to define an important region which ranges from r_1=0.93 bohr to r_2=1.74 bohr. It is indicated in Fig. 2 as hatched area and mainly determines the difference between the slopes $\Delta E_{xc}/\Delta\Omega$ of two functionals and thus the ordering of the lattice constants. In order to gain further insight about the origin of this important region, Fig. 2 also shows $r^2\rho$ for the Li-1s and Li-2s,2p states inside the atomic sphere of lithium. We can easily identify the important region as the region between the Li-1s ("semicore") and 2s,2p (valence) states and corresponding to the atomic shell structure. As long as the Li-1s state (in $r^2\rho$) dominates, both for PBE−AM05 and PBE−PBEsol (to a smaller extent) $\Delta E_{xc}^{F1-F2}(r_{\max})/\Delta\Omega$ increases; but when the Li-2s,2p states gets larger (r_s is larger), $\Delta E_{xc}^{F1-F2}(r_{\max})/\Delta\Omega$ decreases. For AM05, the first part dominates, leading overall to a smaller slope $\Delta E_{xc}/\Delta\Omega$ (see Table II) than PBE, and thus a larger lattice constant. On the other hand, for PBEsol, both regions nearly cancel, which makes PBE and PBEsol lattice constants very similar. It is this region that determines the "size" of an atom and thus the equilibrium lattice constant of the solid, and not the "overlap region" between the valence orbitals centered at different atomic sites.

After having identified the region of space, which is energetically the most important for the determination of the lattice constant, we will study the different contributions to the slope $dE_{xc}/d\Omega$. As briefly discussed above, looking at F_{xc} alone is not enough to understand the trends in the lattice constant for Li, and thus a more systematic study is necessary.

TABLE III. The important region (see text for definition) around the nucleus defined by the interval $[r_1,r_2]$ (r_1 and r_2 are radial distances from the nucleus). $\bar{r}_s$ and $\bar{s}$ are the averages of r_s and s inside $[r_1,r_2]$ at the equilibrium lattice constants. r_1, r_2, and $\bar{r}_s$ are expressed in bohr.

Solid	$[r_1,r_2]$	$\bar{r}_s$	$\bar{s}$
Li	[0.93, 1.74]	2.54	1.51
Na	[1.54, 2.47]	2.90	1.46
K	[1.69, 3.40]	3.17	1.35
Rb	[1.93, 3.68]	3.23	1.37

The exchange-correlation energy density integrated within the important region [defined by r_1 and r_2 and of volume V $=(4/3)\pi(r_2^3-r_1^3)$] can be approximated by considering the averages $\bar{r}_s$ and $\bar{s}$ [Eq. (9)] within V (see Table III),

$$\langle\epsilon_{xc}\rangle_V = \int_V \epsilon_{xc}(r_s(\mathbf{r}),s(\mathbf{r}))d^3r \approx V\epsilon_{xc}(\bar{r}_s,\bar{s}) = -VA\frac{F_{xc}(\bar{r}_s,\bar{s})}{\bar{r}_s^4}, \tag{11}$$

where $A=(3/4)(3/\pi)^{1/3}[3/(4\pi)]^{4/3}$. The derivative of $\langle\epsilon_{xc}\rangle_V$ with respect to the unit-cell volume Ω is given by

$$\frac{d\langle\epsilon_{xc}\rangle_V}{d\Omega} = VA(G_1+G_2+G_3), \tag{12}$$

where

$$G_1 = \left.\frac{4}{r_s^5}\frac{dr_s}{d\Omega}F_{xc}\right|_{r_s=\bar{r}_s,s=\bar{s}}, \tag{13}$$

$$G_2 = \left.-\frac{1}{r_s^4}\frac{\partial F_{xc}}{\partial r_s}\frac{dr_s}{d\Omega}\right|_{r_s=\bar{r}_s,s=\bar{s}}, \tag{14}$$

$$G_3 = \left.-\frac{1}{r_s^4}\frac{\partial F_{xc}}{\partial s}\frac{ds}{d\Omega}\right|_{r_s=\bar{r}_s,s=\bar{s}}. \tag{15}$$

From Eqs. (12)–(15) we can see that $d\langle\epsilon_{xc}\rangle_V/d\Omega$ depends on r_s, s, F_{xc}, and the derivatives $dr_s/d\Omega$, $ds/d\Omega$, $\partial F_{xc}/\partial r_s$, and $\partial F_{xc}/\partial s$. Since we chose to use the same electron density for all functionals, s, r_s, $dr_s/d\Omega$, and $ds/d\Omega$ are also the same for all functionals, and only F_{xc} (in G_1), $\partial F_{xc}/\partial r_s$ (in G_2), and $\partial F_{xc}/\partial s$ (in G_3) differ from one functional to another. Therefore, the differences between the lattice constants obtained by the various functionals are only due to F_{xc} and its derivatives $\partial F_{xc}/\partial r_s$ and $\partial F_{xc}/\partial s$.

Considering, for instance, the experimental unit-cell volume Ω we can use the values of $\bar{r}_s$ and $\bar{s}$ (and their Ω derivatives) to calculate G_1, G_2, and G_3 (results in Table IV). Note that G_2 (related to $\partial F_{xc}/\partial r_s$) is of least importance, while the main contribution comes from G_1 (related to F_{xc}). From G_1 alone, however, one would conclude that LDA should give the largest and PBE the smallest lattice constant, which is not true. Even though G_2 and G_3 (related to $\partial F_{xc}/\partial s$) are two and one order of magnitude smaller than G_1, they are important. Indeed, G_3 does not contribute for

TABLE IV. The values of G_1 [Eq. (13)], G_2 [Eq. (14)], G_3 [Eq. (15)], and their sum G_{tot} for Li and V at the equilibrium geometry. The values are in mRy/bohr^3.

Functional	G_1	G_2	G_3	G_{tot}
		Li		
LDA	0.555	−0.013	−0.000	0.542
PBEsol	0.577	−0.006	−0.079	0.492
WC	0.582	−0.005	−0.096	0.481
AM05	0.584	−0.011	−0.098	0.475
PBE	0.612	−0.005	−0.122	0.486
		V		
LDA	14.456	−0.288	−0.000	14.168
PBEsol	14.527	−0.237	−0.489	13.801
WC	14.668	−0.209	−0.630	13.830
AM05	14.402	−0.254	−0.459	13.690
PBE	14.877	−0.209	−1.256	13.412

LDA and this causes the largest slope $d\langle\epsilon_{xc}\rangle_V/d\Omega$ and thus the smallest lattice constant for LDA. Also, adding G_2 and G_3 to G_1 makes $G_{tot}=G_1+G_2+G_3$ for WC and AM05 smaller than for PBE, which is in agreement with the ordering of the lattice constant of Li (Table I). Overall, the trends in the slopes $\Delta E_{xc}/\Delta\Omega$, and thus the lattice constants, are fairly well reproduced by G_{tot}: LDA and AM05 are the extrema, the others are in between, and WC is between PBE and AM05.

Table III also shows the important region and the averages $\bar{r}_s$ and $\bar{s}$ for the other elements of group IA. Note that the important region is always located in a region separating the outermost core from the valence electrons. Therefore, the distance from the nucleus to the important region is larger for heavier elements. The inner-core electrons do primarily not cause different lattice constants for different functionals. Furthermore, we can see an increase in $\bar{r}_s$ with the nuclear charge Z which stems from the more diffuse orbitals, while $\bar{s}$ is reduced from Li to K (which has a similar values as for Rb).

B. Vanadium

Vanadium has been chosen to represent a $3d$ transition-metal element. According to Table I, all tested functionals lead to too small lattice constants compared to experiment. The relative error of LDA is about 3%, while PBE is the most accurate (less than 1% underestimation). The relative errors of WC, AM05, and PBEsol (which lead to very similar lattice constants) are in between LDA and PBE with about 2% of the relative error. Figure 5 shows the evolution of r_s and s along the shortest path between two V atoms (at the equilibrium geometry). Since vanadium is not a free-electron-like metal as lithium, r_s does not reach a constant value and s is not zero in the interstitial. The reduced density gradient s nicely shows the shell structure of the atom and, similar to Li, a maximum at 1.5 bohr which lies in the range where the $3s,3p$ semicore (but also the $3d$ valence) electrons

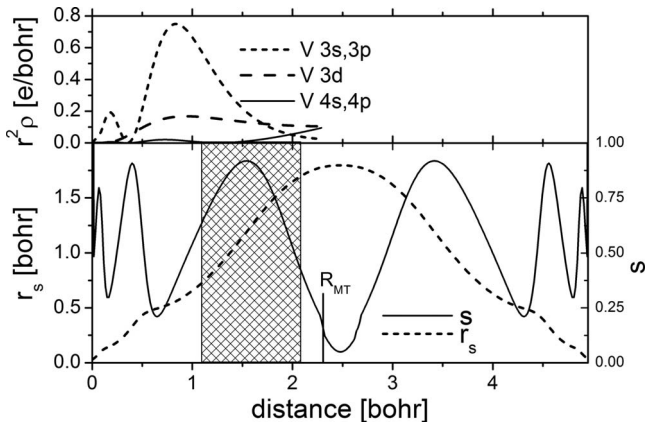

FIG. 5. Top: $r^2\rho$ of $3s$, $3p$ semicore, $3d$, and $4s,4p$ valence states of vanadium (inside the atomic sphere). Bottom: r_s and s along the $(0,0,0)\rightarrow(1/2,1/2,1/2)$ path at the equilibrium lattice constant. The important region (see text for definition) is illustrated by the hatched rectangle from 1.10 to 2.07 bohr and the atomic sphere radius (R_{MT}^V) of the atom at 0 is indicated by a line at 2.29 bohr.

are separated from the $4s,4p$ valence electrons. The maximum value of s, however, is about a factor of 2 smaller than for Li. Also, note that the maxima in the radial density $r^2\rho$ for the semicore $3s,3p$ and the valence $3d$ states fall very close together, but the tails of the $3d$ orbitals are more long ranged. A similar plot for a $5d$ element like tantalum shows that the $5d$ maximum is further out compared to the $5s,5p$ maxima and this difference between a $3d$ and a $5d$ metal may explain the different behavior of the functionals for $3d$ and $5d$ elements, where, e.g., PBE shows a clear underbinding (too large lattice constants) for $5d$, while LDA shows a pronounced overbinding (too small lattice constants) for $3d$ systems.

The same analysis that was done for lithium in the preceding section has been carried out for vanadium. The important region V (i.e., the region where the slopes $\Delta E_{xc}/\Delta\Omega$ of two functionals differ the most) has been identified to be between 1.10 and 2.07 bohr as indicated in Fig. 5, while the interstitial contribution is again nearly zero. An analysis of the different contributions to $d\langle\epsilon_{xc}\rangle_V/d\Omega$ [Eqs. (12)–(15)] at the equilibrium geometry ($\bar{r}_s=1.36$ bohr and $\bar{s}=0.76$ inside V) shows (Table IV) that again G_1 (F_{xc}) is the largest contribution, but the ordering of the equilibrium lattice constants cannot be deduced solely from it. For that purpose it is also necessary to consider G_2 ($\partial F_{xc}/\partial r_s$) and G_3 ($\partial F_{xc}/\partial s$). LDA (PBE) leads to the largest (smallest) values of G_{tot}, while PBEsol, WC, and AM05 lie inside this bound. This ordering reflects the trends observed in the lattice constant. Note that here G_2 and G_3 are of the same order of magnitude, while for lithium G_2 was one order of magnitude smaller than G_3.

C. FeAl

We have chosen FeAl as an example of a metallic binary compound. From Table I, we can see that for the lattice constant the best agreement with experiment is obtained with PBE which slightly underestimates a_0, while the other func-

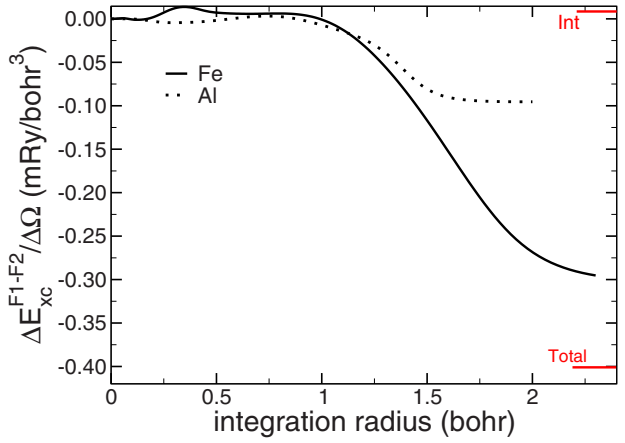

FIG. 6. (Color online) $\Delta E_{xc}^{F1-F2}(r_{\max})/\Delta\Omega$ for FeAl with $F1$ =PBE and $F2$=PBEsol plotted as a function of the integration radius $r_{\max}$. The values of $\Delta E_{xc}^{F1-F2}/\Delta\Omega$ in the interstitial region and the whole unit cell are indicated by "Int" and "Total." The radii of the atomic spheres are $R_{\mathrm{MT}}^{\mathrm{Fe}}=2.3$ bohr and $R_{\mathrm{MT}}^{\mathrm{Al}}=2.0$ bohr.

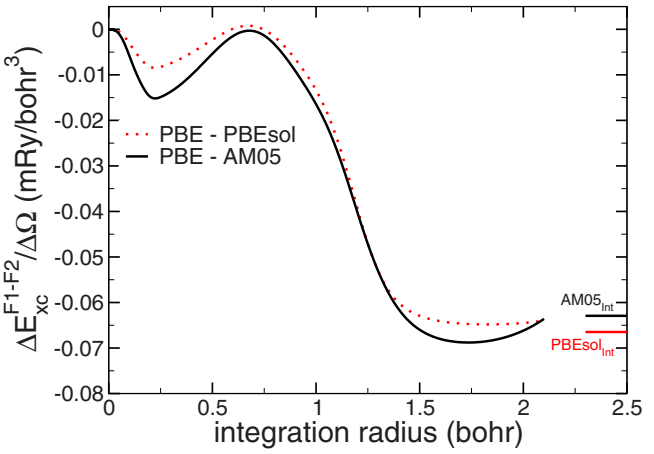

FIG. 7. (Color online) $\Delta E_{xc}^{F1-F2}(r_{\max})/\Delta\Omega$ for silicon with $F1$ =PBE and $F2$=PBEsol (dotted line) and $F1$=PBE and $F2$ =AM05 (solid line) plotted as a function of the integration radius $r_{\max}$. The values of $\Delta E_{xc}^{F1-F2}/\Delta\Omega$ in the interstitial region are indicated by "Int." The radius of the atomic sphere is $R_{\mathrm{MT}}^{\mathrm{Si}}=2.1$ bohr.

tionals lead to very large underestimations. By comparing the FeAl results with the results for the pure elements Fe and Al (see Table I and Fig. 1 of Ref. 28), we can see that the trends in the results for FeAl follow closely the trends for bcc Fe (all functionals underestimate a_0), while for fcc Al, LDA and PBE lead to clear underestimation and overestimation, respectively, and the other functionals yield very accurate lattice constants.

In order to understand why FeAl and Fe show similar trends we investigated the change in slope $\Delta E_{xc}/\Delta\Omega$ between two functionals $(\Delta E_{xc}^{F1-F2}/\Delta\Omega)$ as a function of the integration radius $r_{\max}$ inside the Fe and Al atomic spheres. From Fig. 6, which shows $\Delta E_{xc}^{F1-F2}(r_{\max})/\Delta\Omega$ for the case $F1$=PBE and $F2$=PBEsol (using the PBE electron density), we can see that the important region is between 1 and 2 bohr for Fe (the region of the tails of the $3d$ orbitals as well as the separation between the $3s,3p$ core from $4s$ valence electrons) and between 1.1 and 1.5 bohr for Al. We can also see that the contribution from the Fe sphere is three times larger than the contribution from the Al sphere, which explains the fact that the trends in a_0 for FeAl and pure Fe are very similar. Note that the contribution coming from the interstitial region is almost zero. Finally, we mention that the maximum values of s in the Fe and Al atomic spheres are 0.8 and 1.4, respectively.

D. Silicon

The structures of the solids we have considered so far are fairly close packed, while the one of silicon is open with large empty regions of space. From Table I we can see that the LDA lattice constant is close to the experimental one, while the GGAs (PBE in particular) clearly overestimate a_0. From Fig. 7, which shows the difference in slope between two functionals $\Delta E_{xc}^{F1-F2}(r_{\max})/\Delta\Omega$ for $(F1,F2)$ $=$(PBE,PBEsol) and $(F1,F2)$=(PBE,AM05), we can see that the important region inside the atomic sphere can be clearly estimated to be between 0.7 and 1.5 bohr, while for an integration radius $r_{\max}$ between 1.5 and $R_{\mathrm{MT}}^{\mathrm{Si}}=2.1$ bohr, $\Delta E_{xc}^{F1-F2}(r_{\max})/\Delta\Omega$ is rather constant. The important region corresponds to the separation between $2s,2p$ core and $3s,3p$ valence states. Note that there is little difference between PBEsol and AM05 functionals, which is expected since both functionals lead to quasi-identical lattice constants.

However, as we can see from Fig. 7 and Table V, the interstitial contribution to $\Delta E_{xc}^{F1-F2}/\Delta\Omega$ can be as large as the one from the atomic sphere (in contrast to the previously studied solids) and, in order to understand this, we show a two-dimensional plot of the reduced density gradient s in Fig. 8. Inside the atomic spheres, s becomes as large as 1.3 (in the core-valence separation region), while in the bonding region between two neighboring Si atoms, s is very small. However, in the large empty regions of this open structure, the tails of the valence orbitals lead to an increase in s up to 0.9. Thus, these large interstitial regions with relatively large values of s lead to a value of $\Delta E_{xc,\mathrm{int}}^{F1-F2}/\Delta\Omega$ of the same order as $\Delta E_{xc,\mathrm{sph}}^{F1-F2}/\Delta\Omega$ (Table V). We mention that for isostructural heavier materials such as Ge or GaAs, the maximum value of s in the core-valence region is smaller (e.g., 0.9 in GaAs) than in Si, but larger in the interstitial region (e.g., 1.2 for GaAs). The fact that s is larger in the interstitial region can explain why in the series C, Si, Ge, GaAs, the PBE lattice constants get worse (more pronounced overestimation) for

TABLE V. The difference in slope $\Delta E_{xc}^{F1-F2}/\Delta\Omega$ between two functionals $F1$ and $F2$ for silicon. The total value is decomposed into the contributions coming from the atomic spheres and the interstitial region. The values are in mRy/bohr^3.

$F1-F2$	$\frac{\Delta E_{xc}^{F1-F2}}{\Delta\Omega}$	$\frac{\Delta E_{xc,\mathrm{sph}}^{F1-F2}}{\Delta\Omega}$	$\frac{\Delta E_{xc,\mathrm{int}}^{F1-F2}}{\Delta\Omega}$
PBE−LDA	−0.245	−0.180	−0.065
PBE−PBEsol	−0.131	−0.064	−0.066
PBE−WC	−0.136	−0.071	−0.065
PBE−AM05	−0.127	−0.064	−0.063

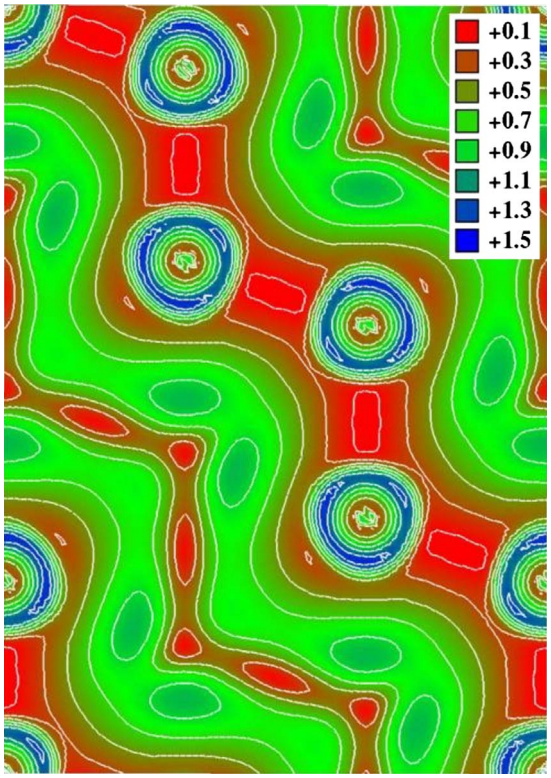

FIG. 8. (Color online) Two-dimensional plot of the reduced density gradient s in silicon in the (110) plane.

heavier elements. Indeed, the larger s gets in the interstitial region, the more the unit cell will expand, because larger values of s cause more negative exchange-correlation energies and thus a larger equilibrium volume.

E. LiF

LiF is a solid where adding gradient corrections to LDA dramatically increases the lattice constant, similar to Li (see Table I). Actually, Li and LiF are solids for which the difference between the relative errors of LDA and the *softest* GGA is among the largest in a testing set of 60 solids (see Fig. 1 of Ref. 28).

From the analysis of $\Delta E_{xc}^{F1-F2}/\Delta\Omega$ and its spatial partitioning into the atomic ($R_{\mathrm{MT}}^{\mathrm{Li}}=1.5$ bohr and $R_{\mathrm{MT}}^{\mathrm{F}}=2.07$ bohr) and interstitial regions, we can identify the important regions for LiF. We observe that the contributions to $\Delta E_{xc}^{F1-F2}/\Delta\Omega$ coming from inside the Li and F atomic spheres are on the same order of magnitude and, depending on the considered functionals $F1$ and $F2$, may have the same or opposite sign (see the bottom panel of Fig. 9). Inside the Li atomic sphere, the important region is (as in the case of metallic bcc Li) within a distance of 1–1.5 bohr from the nucleus and comes from the tails of the Li-1s semicore state. However, the Li-1s density is modified compared to metallic Li such that its contribution to the slope is about twice as large (compare Figs. 4 and 9). Inside the F sphere there is a first important region between 0.1 and 0.4 bohr, where the F-1s core states dominate. For larger distances where the valence charge density (F-2s,2p see the middle panel of Fig. 9) dominates, the F contributions to $\Delta E_{xc}^{F1-F2}/\Delta\Omega$ do not show much structure for most pairs of functionals $F1$ and $F2$. Similarly as in Si, the interstitial contribution is very important and can even be up to 10 times as large as the contributions from within the atomic spheres. The electron density in the interstitial region originates from the tails of the F-2p electrons (the F-2p radial density $r^2\rho$ is still large at $R_{\mathrm{MT}}^{\mathrm{F}}=2.07$ bohr; see Fig. 9) and this contributes significantly to $\Delta E_{xc}^{F1-F2}/\Delta\Omega$.

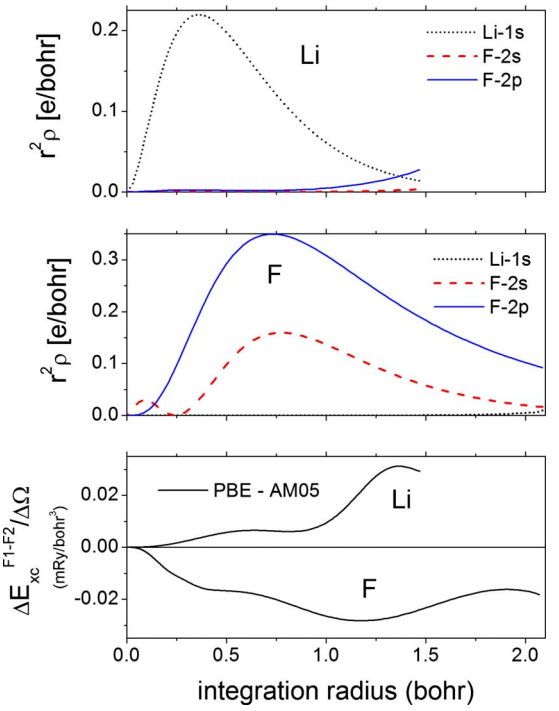

FIG. 9. (Color online) $r^2\rho$ inside the Li (top panel) and F (middle panel) atomic spheres of Li-1s (semi)core and F-2s and F-2p valence states in LiF. Bottom: $\Delta E_{xc}^{F1-F2}(r_{\max})/\Delta\Omega$ for LiF with $F1$=PBE and $F2$=AM05 as a function of the integration radius $r_{\max}$. Note that the contribution to the slope from the interstitial is much larger (–0.10 mRy/bohr^3).

Figure 10 shows the reduced density gradient s in the (110) plane. We can see that, inside the Li atomic sphere, the largest values of s occur at distances between $r_1=1$ bohr and $r_2=1.5$ bohr from the nucleus, which was determined to be one of the important regions. Around the F atom, the largest values of s (the green region) start at about 1 bohr from the nucleus and extend beyond the atomic sphere of F, which is the main reason why for LiF also the interstitial region is important.

F. Graphite

In graphite, the carbon atoms which lie in the same hexagonal plane are covalently bound, while the interactions between atoms belonging to different planes are noncovalent and thus weak. It is well known that the attractive London dispersion forces, which can be the dominant component in the interaction energy for such system, are not taken into account by semilocal functionals, and that this missing dispersion interaction is sometimes (depending on the func-

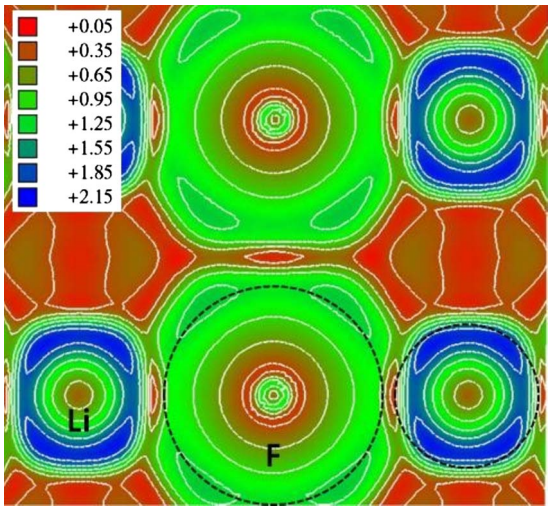

FIG. 10. (Color online) Two-dimensional plot of the reduced density gradient s in LiF in the (110) plane. The atomic sphere radii ($R_{MT}^{Li}=1.5$ bohr and $R_{MT}^{F}=2.07$ bohr) are indicated by dashed circles.

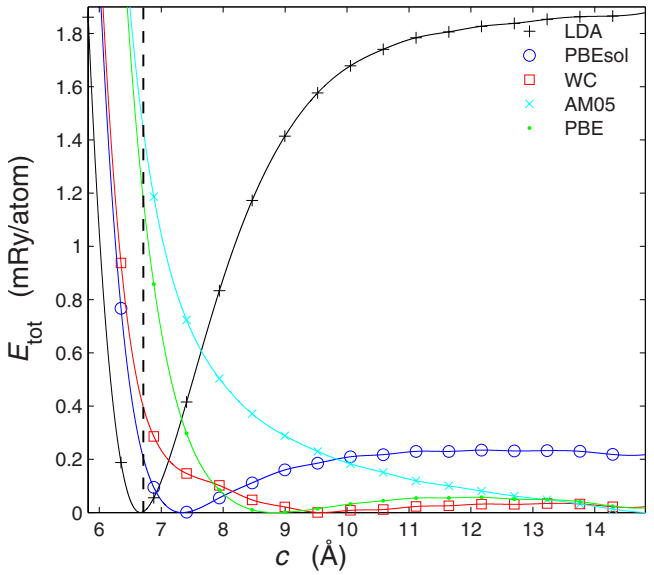

FIG. 11. (Color online) Total energy of graphite vs the lattice constant c (the interlayer distance is $c/2$). The in-plane lattice constant a was kept fixed at the experimental value (2.464 Å) for all values of c. The minimum for the AM05 functional is either much larger than 15 Å or absent. The vertical dashed line represents the experimental lattice constant ($c_0=6.71$ Å).

tional and the system under consideration) "replaced" with an artificial attraction that arises due to the nonzero overlap between the two weakly interacting fragments (e.g., two hexagonal planes). However, the results obtained with semilocal functionals for such weakly bound systems are very often quantitatively wrong and this is the reason why functionals especially designed for such systems have been proposed (see, e.g., Refs. 69 and 70).

The lattice constant c (the interlayer distance is $c/2$) of graphite was optimized,[28] while the in-plane lattice constant a was kept fixed at the experimental value (2.464 Å). From the results shown in Table I and Fig. 11, we can see that a very broad range of equilibrium values of c are found with the different functionals. LDA yields a very good value for c_0, and PBEsol is still rather accurate in comparison to the other GGA functionals that perform very badly. For instance, AM05 does not show any binding between the graphene layers.

A two-dimensional plot of s in a plane normal to the hexagonal layers is shown in Fig. 12. We can see maxima of s inside the carbon spheres and also in the interstitial region between two hexagonal planes. Due to symmetry, minima appear at mid-distance between two hexagonal planes, and within the hexagonal plane there is a large region of small s in the bonding region between two C atoms.

Figure 13 shows, for the equilibrium structure ($c_0=6.71$ Å$=12.68$ bohr), the one-dimensional curves of r_s and s along the path indicated with a black dotted line in Fig. 12 (one C atom is at 0 and the second is at 6.34 bohr). We can observe the shell structure (the separation between the $1s$ and $2s$ shells) of the C atom which leads to a peak of s at ~ 0.4 bohr from the nucleus. For distances >0.9 bohr, s increases but decreases again at 2.2 bohr due to symmetry reasons right in the middle between the two C atoms.

Figure 13 also shows r_s and s along the same path, but for a stretched lattice constant $c=10.05$ Å$=19$ bohr. An increase in the r_s maximum up to 9.8 bohr is noticed and also s increases up to nearly 3.5. It was already known in the literature[71,72] that the GGA functionals whose enhancement factors F_{xc} violate the Lieb-Oxford bound[49] (because $F_{xc}\to\infty$ for $s\to\infty$) give very shallow or no minimum in potential-energy surfaces of weakly bound systems, which is the case of the AM05 functional. The steady increase (i.e., divergence) in F_{xc}^{AM05} with s (see Fig. 1) energetically favors a larger c (the isolated graphene layers are favored) and in the cases of weak interactions this effect has a much stronger impact than in the case of strong (e.g., covalent) interactions.

From Fig. 11 we can also see that PBEsol and WC results are very similar for $c<7$ Å, which is also in agreement with Fig. 1, where we can see that F_{xc}^{PBEsol} and F_{xc}^{WC} are very similar for $s<1.5$. At larger c the WC results resemble more the PBE results (showing just a very slight minimum), which is again explainable since the larger s gets, the closer are F_{xc}^{PBE} and F_{xc}^{WC}.

IV. DISCUSSION AND SUMMARY

Before coming to the summary of our work, we would like to briefly make a short review of previous papers that also present analyses of semilocal functionals. Extensive analyses of the effect of gradient corrections of GGA functionals were done by Perdew and collaborators in Refs. 34–37. They made a very detailed study of r_s, s, and the relative spin polarization $\zeta=(\rho_\uparrow-\rho_\downarrow)/(\rho_\uparrow+\rho_\downarrow)$ in atoms, molecules, surfaces, and solids. For their analyses, they used energy-weighted averages of r_s, s, and ζ [see Eq. (6) of Ref. 34] and considered the variation of these averages with respect to the bond length or lattice constant. They also made use of distribution functions of r_s, s, and ζ [see Eq. (4) of

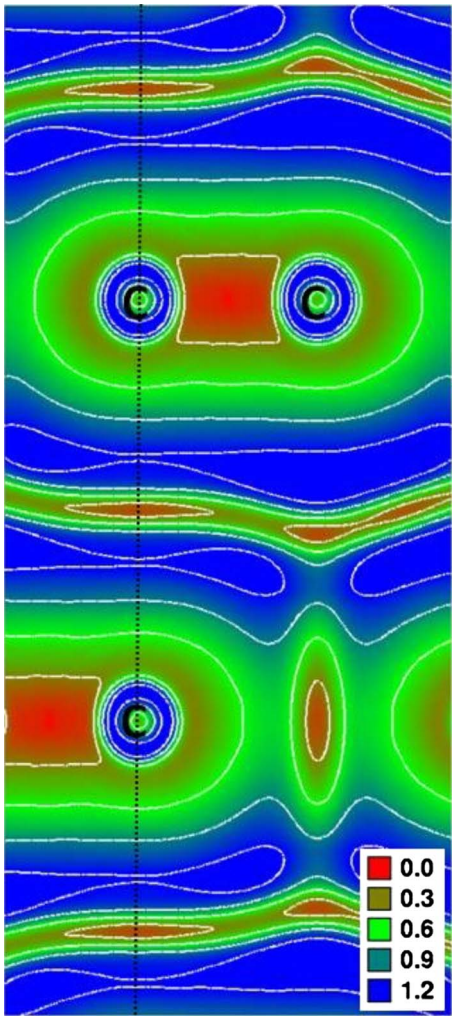

FIG. 12. (Color online) Two-dimensional plot of the reduced density gradient s in graphite within a plane normal to the hexagonal layers.

Ref. 35]. From their analyses, they were able to explain trends like, for instance, why adding the gradient correction shortens the H_2 bond length,[34] while usually the bond lengths are elongated when a gradient correction is added. More generally, adding gradient corrections will favor two changes: denser electron density (i.e., shorter bond lengths) and more inhomogeneity in the electron density (i.e., larger bond lengths). Only in a few cases (e.g., H_2) the first change will win. The analysis we have made and the analyses of Perdew and collaborators have similarities, but ours were more aimed at explaining the results for the equilibrium lattice constants of solids.

In Ref. 33, Philipsen and Baerends tested GGA functionals for the calculation of the cohesive energy of 3d transition metals and a detailed analysis of the GGA functionals was done for Cu. First, they showed that the LDA exchange-correlation contribution to the cohesive energy of Cu is repulsive in the atomic region and attractive in the bonding region. Then, they observed that the main effect of adding gradient correction is to reduce the attractiveness of exchange correlation in the bonding region. Another conclusion of their work is that (for Cu) the regions of space with

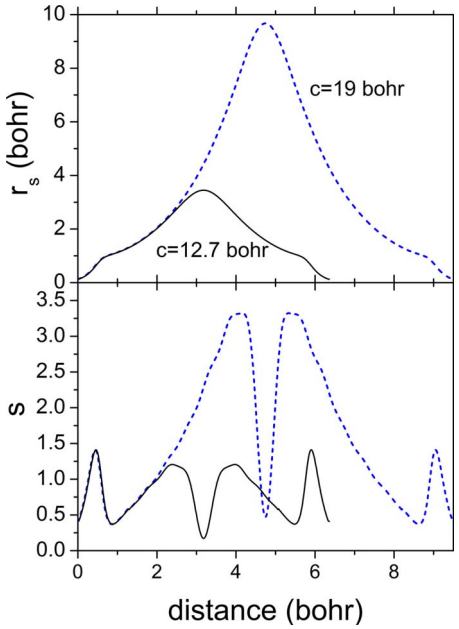

FIG. 13. (Color online) One-dimensional plot of r_s (top) and s (bottom) in graphite at the experimental equilibrium geometry (c_0 =6.71 Å=12.68 bohr) (black solid lines) and at a stretched geometry (c=10.05 Å=19 bohr) (blue dashed lines) from one C atom to the next along the c axis (the path is indicated with a black dotted line in Fig. 12).

$s<0.2$ do not contribute to the gradient correction.

From the analyses of Fuchs *et al.*[38] and Ruban and Abrikosov[40] on solids, it was concluded that the region of core-valence overlap is of great importance—a conclusion that is also supported by our analysis on Li and V, for instance. In a recent study on the performance of semilocal functionals on solids, Csonka *et al.*[29] showed a correlation between the maximum values of s in solids and the difference in results between PBEsol and AM05 functionals. While AM05 and PBEsol give similar results for solids with small value of the maximum of s (e.g., 4d transition metals), it is not the case for solids with larger maximum of s (ionic solids and alkali metals).

In their analyses, Mattsson and collaborators (see Ref. 73 and references therein) pointed out the need to take into account the different amounts of surface between two different structures when their energies (calculated with common semilocal functionals) are compared. Their definition of "surface" also includes *internal* surfaces like, for example, the surface around the large interstitial region in Si.[73] Related to this concept of surfaces, we mention the study of Stroppa and Kresse[74] of the adsorption of the CO molecule on the late 4d and 5d transition-metal surfaces. From their results, they concluded that there is no semilocal functional that is able to yield accurate results for different properties (structural and energetical) and types of systems (finite and infinite) at the same time.

In the present work, the spatial distribution of the Wigner-Seitz radius r_s and reduced density gradient s has been studied in selected solids. We considered lithium (which is close to the homogeneous electron gas), vanadium (a 3d transition

metal), FeAl (an intermetallic compound), silicon (a semiconductor), LiF (an ionic insulator), and graphite (whose hexagonal layers are bound by weak interactions). We have identified which region in space is energetically important for the structural properties. For this purpose we studied the variation of the exchange-correlation energy with respect to the unit-cell volume. For all systems the important region includes a radial shell around the atoms, which separates the semicore from the valence electrons. For open structures such as silicon or graphite, but also inhomogeneous systems like ionic compounds (e.g., MgO or LiF), also the interstitial region is important since even small contributions (from the tails of the atomic densities) will sum up over a large volume.

Using the averages of r_s and s in the energetically important region, a better understanding of the "unusual trends" in the lattice constants (e.g., in lithium) could be obtained. It turns out that it is not only the value of the enhancement factor F_{xc}, but also its derivatives with respect to r_s and s which determine the equilibrium lattice constant.

Further, during our analysis we noticed that, in the considered solids, values of s larger than 1.5 (2 for light alkali metals) and values of r_s larger than 4 bohr (7 bohr for stretched graphite) do not occur. Therefore, it is $F_{xc}(r_s,s)$ (and its r_s and s derivatives) up to these values of r_s and s which determines the geometry of solids, while the behavior of $F_{xc}(r_s,s)$ for larger r_s and s is completely unimportant. Note that this statement is not true for cohesive energies and the geometry of finite systems (molecules).

To conclude, we think that the general limits of accuracy of semilocal exchange-correlation functionals have not yet been reached. Nevertheless, to improve the geometry of solids over the currently best GGAs (e.g., WC, PBEsol, or AM05) it will be necessary to consider more sophisticated semilocal functionals, which may lead to improvements for cases where functionals such as PBEsol, WC, or AM05 still have large errors (e.g., $3d$ or heavy alkali-earth metals). Meta-GGAs,[30–32] which due to the use of the kinetic-energy density are more flexible (but still of the semilocal form), could give an improvement (see, e.g., Ref. 75); but, until now, only a few such meta-GGA functionals have been proposed and there is room for improvement. An analysis like the one done in the present work, but including also the kinetic-energy density, could certainly help in deriving more accurate meta-GGA functionals.

ACKNOWLEDGMENTS

We are grateful to John P. Perdew and Gábor I. Csonka for helpful comments on the manuscript. This work was supported by Project No. P20271-N17 of the Austrian Science Fund and Project No. WP 15 of the Austrian Grid.

[1] P. Hohenberg and W. Kohn, Phys. Rev. **136**, B864 (1964).
[2] W. Kohn and L. J. Sham, Phys. Rev. **140**, A1133 (1965).
[3] P. Mori-Sánchez, Q. Wu, and W. Yang, J. Chem. Phys. **123**, 062204 (2005).
[4] J. Harl and G. Kresse, Phys. Rev. Lett. **103**, 056401 (2009).
[5] A. D. Becke, J. Chem. Phys. **98**, 5648 (1993).
[6] J. P. Perdew, V. N. Staroverov, J. Tao, and G. E. Scuseria, Phys. Rev. A **78**, 052513 (2008).
[7] S. Grimme, J. Chem. Phys. **124**, 034108 (2006).
[8] A. J. Cohen, P. Mori-Sánchez, and W. Yang, J. Chem. Phys. **127**, 034101 (2007).
[9] T. Benighaus, R. A. DiStasio, Jr., R. C. Lochan, J.-D. Chai, and M. Head-Gordon, J. Phys. Chem. A **112**, 2702 (2008).
[10] E. R. Johnson and A. D. Becke, J. Chem. Phys. **128**, 124105 (2008).
[11] F. Corà, M. Alfredsson, G. Mallia, D. S. Middlemiss, W. C. Mackrodt, R. Dovesi, and R. Orlando, Struct. Bonding (Berlin) **113**, 171 (2004).
[12] J. Heyd, J. E. Peralta, G. E. Scuseria, and R. L. Martin, J. Chem. Phys. **123**, 174101 (2005).
[13] J. Paier, M. Marsman, K. Hummer, G. Kresse, I. C. Gerber, and J. G. Ángyán, J. Chem. Phys. **124**, 154709 (2006); **125**, 249901 (2006).
[14] S. Kümmel and L. Kronik, Rev. Mod. Phys. **80**, 3 (2008).
[15] I. C. Gerber, J. G. Ángyán, M. Marsman, and G. Kresse, J. Chem. Phys. **127**, 054101 (2007).
[16] J. P. Perdew, J. A. Chevary, S. H. Vosko, K. A. Jackson, M. R. Pederson, D. J. Singh, and C. Fiolhais, Phys. Rev. B **46**, 6671 (1992); **48**, 4978(E) (1993).
[17] J. P. Perdew, K. Burke, and M. Ernzerhof, Phys. Rev. Lett. **77**, 3865 (1996); **78**, 1396 (1997).
[18] R. Armiento and A. E. Mattsson, Phys. Rev. B **72**, 085108 (2005).
[19] Z. Wu and R. E. Cohen, Phys. Rev. B **73**, 235116 (2006); Y. Zhao and D. G. Truhlar, *ibid.* **78**, 197101 (2008); Z. Wu and R. E. Cohen, *ibid.* **78**, 197102 (2008).
[20] J. P. Perdew, A. Ruzsinszky, G. I. Csonka, O. A. Vydrov, G. E. Scuseria, L. A. Constantin, X. Zhou, and K. Burke, Phys. Rev. Lett. **100**, 136406 (2008); **102**, 039902(E) (2009); A. E. Mattsson, R. Armiento, and T. R. Mattsson, *ibid.* **101**, 239701 (2008); J. P. Perdew, A. Ruzsinszky, G. I. Csonka, O. A. Vydrov, G. E. Scuseria, L. A. Constantin, X. Zhou, and K. Burke, *ibid.* **101**, 239702 (2008).
[21] Y. Zhao and D. G. Truhlar, J. Chem. Phys. **128**, 184109 (2008).
[22] A. Ruzsinszky, G. I. Csonka, and G. E. Scuseria, J. Chem. Theory Comput. **5**, 763 (2009).
[23] L. S. Pedroza, A. J. R. da Silva, and K. Capelle, Phys. Rev. B **79**, 201106(R) (2009).
[24] G. K. H. Madsen, Phys. Rev. B **75**, 195108 (2007).
[25] F. Tran, R. Laskowski, P. Blaha, and K. Schwarz, Phys. Rev. B **75**, 115131 (2007).
[26] A. E. Mattsson, R. Armiento, J. Paier, G. Kresse, J. M. Wills, and T. R. Mattsson, J. Chem. Phys. **128**, 084714 (2008).
[27] M. Ropo, K. Kokko, and L. Vitos, Phys. Rev. B **77**, 195445 (2008).
[28] P. Haas, F. Tran, and P. Blaha, Phys. Rev. B **79**, 085104 (2009); **79**, 209902(E) (2009).
[29] G. I. Csonka, J. P. Perdew, A. Ruzsinszky, P. H. T. Philipsen, S.

Lebègue, J. Paier, O. A. Vydrov, and J. G. Ángyán, Phys. Rev. B **79**, 155107 (2009).
[30] J. P. Perdew, S. Kurth, A. Zupan, and P. Blaha, Phys. Rev. Lett. **82**, 2544 (1999); **82**, 5179 (1999).
[31] J. Tao, J. P. Perdew, V. N. Staroverov, and G. E. Scuseria, Phys. Rev. Lett. **91**, 146401 (2003).
[32] J. P. Perdew, A. Ruzsinszky, G. I. Csonka, L. A. Constantin, and J. Sun, Phys. Rev. Lett. **103**, 026403 (2009).
[33] P. H. T. Philipsen and E. J. Baerends, Phys. Rev. B **54**, 5326 (1996).
[34] A. Zupan, K. Burke, M. Ernzerhof, and J. P. Perdew, J. Chem. Phys. **106**, 10184 (1997).
[35] A. Zupan, J. P. Perdew, K. Burke, and M. Causà, Int. J. Quantum Chem. **61**, 835 (1997).
[36] A. Zupan, P. Blaha, K. Schwarz, and J. P. Perdew, Phys. Rev. B **58**, 11266 (1998).
[37] J. P. Perdew, M. Ernzerhof, A. Zupan, and K. Burke, J. Chem. Phys. **108**, 1522 (1998).
[38] M. Fuchs, M. Bockstedte, E. Pehlke, and M. Scheffler, Phys. Rev. B **57**, 2134 (1998).
[39] V. Tognetti, P. Cortona, and C. Adamo, J. Chem. Phys. **128**, 034101 (2008).
[40] A. V. Ruban and I. A. Abrikosov, Rep. Prog. Phys. **71**, 046501 (2008).
[41] P. A. M. Dirac, Proc. Cambridge Philos. Soc. **26**, 376 (1930).
[42] J. P. Perdew and Y. Wang, Phys. Rev. B **45**, 13244 (1992).
[43] D. M. Ceperley and B. J. Alder, Phys. Rev. Lett. **45**, 566 (1980).
[44] J. P. Perdew and Y. Wang, Phys. Rev. B **33**, 8800 (1986).
[45] J. P. Perdew, Phys. Rev. B **33**, 8822 (1986); **34**, 7406 (1986).
[46] A. D. Becke, Phys. Rev. A **38**, 3098 (1988).
[47] C. Lee, W. Yang, and R. G. Parr, Phys. Rev. B **37**, 785 (1988).
[48] F. A. Hamprecht, A. J. Cohen, D. J. Tozer, and N. C. Handy, J. Chem. Phys. **109**, 6264 (1998).
[49] E. H. Lieb and S. Oxford, Int. J. Quantum Chem. **19**, 427 (1981).
[50] P. R. Antoniewicz and L. Kleinman, Phys. Rev. B **31**, 6779 (1985).
[51] Y. Zhang and W. Yang, Phys. Rev. Lett. **80**, 890 (1998).
[52] E. L. Peltzer y Blancá, C. O. Rodríguez, J. Shitu, and D. L. Novikov, J. Phys.: Condens. Matter **13**, 9463 (2001).
[53] X. Xu and W. A. Goddard III, J. Chem. Phys. **121**, 4068 (2004).
[54] F. D. Vila, J. J. Rehr, H. H. Rossner, and H. J. Krappe, Phys. Rev. B **76**, 014301 (2007).
[55] B. Hammer, L. B. Hansen, and J. K. Nørskov, Phys. Rev. B **59**, 7413 (1999).
[56] C. Adamo and V. Barone, J. Chem. Phys. **116**, 5933 (2002).
[57] J. J. Mortensen, K. Kaasbjerg, S. L. Frederiksen, J. K. Nørskov, J. P. Sethna, and K. W. Jacobsen, Phys. Rev. Lett. **95**, 216401 (2005).
[58] A. D. Becke, J. Chem. Phys. **84**, 4524 (1986).
[59] P. S. Svendsen and U. von Barth, Phys. Rev. B **54**, 17402 (1996).
[60] J. P. Perdew, L. A. Constantin, E. Sagvolden, and K. Burke, Phys. Rev. Lett. **97**, 223002 (2006).
[61] A. E. Mattsson and R. Armiento, Phys. Rev. B **79**, 155101 (2009).
[62] W. Kohn and A. E. Mattsson, Phys. Rev. Lett. **81**, 3487 (1998).
[63] A. B. Alchagirov, J. P. Perdew, J. C. Boettger, R. C. Albers, and C. Fiolhais, Phys. Rev. B **63**, 224115 (2001).
[64] V. N. Staroverov, G. E. Scuseria, J. Tao, and J. P. Perdew, Phys. Rev. B **69**, 075102 (2004); **78**, 239907(E) (2008).
[65] P. Blaha, K. Schwarz, G. K. H. Madsen, D. Kvasnicka, and J. Luitz, WIEN2K: *An Augmented Plane Wave and Local Orbitals Program for Calculating Crystal Properties* (Vienna University of Technology, Austria, 2001).
[66] D. J. Singh and L. Nordström, *Planewaves, Pseudopotentials and the LAPW Method*, 2nd ed. (Springer, New York, 2006).
[67] E. Sjöstedt, L. Nordström, and D. J. Singh, Solid State Commun. **114**, 15 (2000).
[68] G. K. H. Madsen, P. Blaha, K. Schwarz, E. Sjöstedt, and L. Nordström, Phys. Rev. B **64**, 195134 (2001).
[69] M. Dion, H. Rydberg, E. Schröder, D. C. Langreth, and B. I. Lundqvist, Phys. Rev. Lett. **92**, 246401 (2004); **95**, 109902(E) (2005).
[70] S. Grimme, J. Antony, T. Schwabe, and C. Mück-Lichtenfeld, Org. Biomol. Chem. **5**, 741 (2007).
[71] T. A. Wesolowski, O. Parisel, Y. Ellinger, and J. Weber, J. Phys. Chem. A **101**, 7818 (1997).
[72] Y. Zhang, W. Pan, and W. Yang, J. Chem. Phys. **107**, 7921 (1997).
[73] A. E. Mattsson, R. R. Wixom, and R. Armiento, Phys. Rev. B **77**, 155211 (2008).
[74] A. Stroppa and G. Kresse, New J. Phys. **10**, 063020 (2008).
[75] L. Ferrighi, B. Hammer, and G. K. H. Madsen, J. Am. Chem. Soc. **131**, 10605 (2009).